PAPER

Check for updates

A self-indicating and antibacterial gelatine–chitosan blended hydrogel enabling real-time quality control and sustained bioactive agent delivery

Wing-Fu Lai, [iD] †*[ab] Obireddy Sreekanth Reddy, [iD] †[c] Lucy Law,[b] Haicui Wu[b] and Wing-Tak Wong[b]

Hydrogels are one type of materials that are widely exploited for bioactive agent delivery, partly owing to their high biocompatibility and low toxicity. When hydrogels are used as carriers, their performance in agent loading and sustained agent release are predominately determined by the gel structure, which can be largely affected by variations during gel preparation. Till now, effective and easy methods to enable monitoring of such variations in real time have been lacking, making quality control of the generated gel-based carrier technically challenging. To address this technical gap, in this study we take advantage of the clusteroluminogenic properties of gelatine and chitosan to generate a crosslinked blended hydrogel which not only shows intrinsic antibacterial properties and high tunability in delivery performance but also shows a self-indicating capacity to enable quality control during hydrogel preparation. Upon fitting the curves of agent release into different kinetic models, the release profiles of the agent-loaded gels have been found to follow the Higuchi model well, with the non-Fickian mechanism being the major mechanism of the release process. Along with their high efficiency in agent loading, our gels warrant further exploitation for use in bioactive agent delivery and related biomedical applications.

1. Introduction

Hydrogels are swellable networks which can absorb a substantial amount of fluids.[1,2] Their major constituents are polymers, which can be either synthetic or natural in origin. Owing to their high biocompatibility and low toxicity,[3–5] hydrogels are one type of materials that are widely exploited for bioactive agent delivery. When hydrogels are used as carriers, their performance in agent loading and sustained agent release are predominately determined by the gel structure, which can be largely affected by variations during gel preparation. For example, a slight change in the mass-to-mass ratio of the polymer constituents of a polyelectrolyte complex gel could lead to a substantial change in the efficiency in drug encapsulation.[6] Variations in the molecular weight of a gel-forming polymer can also result in alterations in drug release sustainability.[7] Despite the impact of preparation variations on gel performance, till now effective and easy methods to enable monitoring of such

variations in real time are lacking, making quality control of the generated gel-based carrier technically challenging.

To address this technical gap, the objective of this study is to develop a self-indicating hydrogel that enables real-time quality control during gel preparation. Gelatine (GE) is one of the major constituents of the blended gel in this study. It is a hydrolysis product of collagen,[8–10] but compared to collagen, it exhibits higher aqueous solubility and lower antigenicity.[11] Over the years, GE-based hydrogels have been extensively used in bioactive agent delivery.[12–16] For instance, an earlier study has achieved sustained release of basic fibroblast growth factor (bFGF) by using a GE hydrogel, and has successfully led to regenerative effects on acute vocal fold scarring *in vivo*.[17] More recently, carbon dot cross-linked GE nanocomposite hydrogel has also been reported for pH-sensing and pH-responsive delivery of bioactive agents.[18] All these have demonstrated the practical potential of GE in pharmaceutical formulation. In this study, we take advantage of high biocompatibility of GE, along with its clusteroluminogenic properties, to generate a blended hydrogel with chitosan (CS), which is a linear polysaccharide consisting of $\beta(1 \rightarrow 4)$ linked D-glucosamine residues with a variable number of randomly distributed *N*-acetyl-D-glucosamine units and can be derived from chitin *via* alkaline hydrolysis with an inorganic base.[19,20] After the incorporation of CS into the GE-based hydrogel, not only can the properties of

[a]Department of Urology, Zhejiang Provincial People's Hospital, Affiliated People's Hospital, Hangzhou Medical College, Zhejiang 310012, China. E-mail: rori0610@graduate.hku.hk

[b]Department of Applied Biology and Chemical Technology, Hong Kong Polytechnic University, Hong Kong Special Administrative Region, China

[c]Department of Chemistry, Sri Krishnadevaraya University, Anantapur 515003, India

† These authors contribute equally to this article.

the gel be tuned for bioactive agent delivery, but the cluster-oluminogenic properties of the gel enables easy and real-time quality control during hydrogel preparation and hence allows better control of the subsequent performance in agent release. Along with their high efficiency in agent loading and intrinsic antibacterial properties, our gels warrant further exploitation for use in bioactive agent delivery and related biomedical applications.

2. Experimental

2.1 Materials

GE and various other chemicals were purchased from Macklin Chemical Co., Ltd (Shanghai, China). Dulbecco's Modified Eagle's Medium (DMEM; Gibco, Grand Island, USA), penicillin G-streptomycin sulphate (Life Technologies Corporation. USA), and foetal bovine serum (FBS; Hangzhou Sijiqing Biological Engineering Materials Co., Ltd, China) were used as the cell culture medium. Trypsin–EDTA (0.25% trypsin–EDTA) was obtained from Invitrogen (Carlsbad, CA, USA).

2.2 Gel preparation

CS was dissolved in a 5% (v/v) acetic acid solution to generate a 5% (w/v) CS solution. After that, GE was dissolved in water at 50 °C to prepare a 5% (w/v) GE solution. 50 mL of the GE solution was mixed with 50 mL of the CS solution, followed by the addition of 10 mL of glutaraldehyde. The reaction mixture was incubated at ambient conditions until the completion of the gelation process. The gel formed was designated as G050. Other gels (*viz.*, G000, G025, G075 and G100) were prepared based on the volumes as presented in Table 1.

2.3 Thermogravimetric analysis (TGA) and derivative thermogravimetry (DTG)

TGA and DTG of G100, G050 and G000 were performed using a Q50 TGA analyser (TA Instruments, New Castle, Delaware, USA) equipped with platinum pans. Analysis was performed in an inert nitrogen atmosphere from 40 °C to 600 °C. The heating rate was set as 10 °C min^{-1}.

2.4 X-ray diffraction (XRD) analysis

Powder XRD patterns of G100, G050 and G000 were obtained using an X-ray diffractometer (X'Pert PRO, PANalytical Company, Almelo, Netherlands) with CuKα radiation (λ = 1.54060 Å) at a counting rate of 5° min^{-1}.

2.5 Fourier-transform infrared (FT-IR) spectroscopy

FT-IR spectroscopy was carried out using an FT-IR spectrometer (Spectrum 2000; PerkinElmer, Norwalk, CT, USA) at ambient conditions. The potassium bromide (KBr) disk technique was adopted for analysis. Spectra were obtained at a resolution of 2 cm^{-1}, and reported as an average of 16 scans.

2.6 Compressive strength test

The mechanical properties of G000, G025, G050, G075 and G100 were studied using a Universal Testing Machine (Testometric Co. Ltd, Rochdale, UK) as previously described.[6] In brief, all gels were prepared in the shape of a column (diameter = 2.8 cm, height = 1.5 cm). Each of them was placed between the self-levelling plates, and was compressed at a rate of 10 mm min^{-1}.

2.7 Microscopic examination and UV irradiation

Microstructures of the gels were examined under a stereomicroscope, and photographed using a digital microscope camera. Fluorescence images of the gels were captured, after excitation of the gels at 365 nm, by using a small compact digital camera. Photoluminescence (PL) measurements were performed by using a FLS920P fluorescence spectrometer (Edinburgh Instruments Ltd, Livingston, UK).

2.8 Evaluation of swelling ratios

Gels with different mass percentages of CS were prepared and dried in an oven at 60 °C for 24 hours. The swelling properties of the dried gels were determined as previously described.[21] The swelling ratio was calculated using the following equation (eqn (1)):

$$\text{Swelling ratio} = \frac{m_s}{m_d} \tag{1}$$

where m_s and m_d represent the mass of the swollen gel and the mass of the dried gel, respectively.

2.9 Determination of the encapsulation efficiency (EE)

Minocycline hydrochloride (MH) was used as a model agent. Gels with different mass percentages of CS were prepared as usual but MH was added to the reaction mixture at a concentration of 9.17×10^{-6} mol mL^{-1} prior to gelation. The concentration of unloaded MH was determined using ultraviolet-visible (UV-Vis) spectroscopy at λ_{max} of 350 nm. The EE was estimated using the following equation (eqn (2)):

$$\text{EE (\%)} = \frac{m_l}{m_t} \times 100\% \tag{2}$$

where m_l is the mass of MH encapsulated successfully by the gel, and m_t is the total mass of MH added during the encapsulation process.

Table 1 Volumes of the CS solution, GE solution and glutaraldehyde used in preparation of different gels

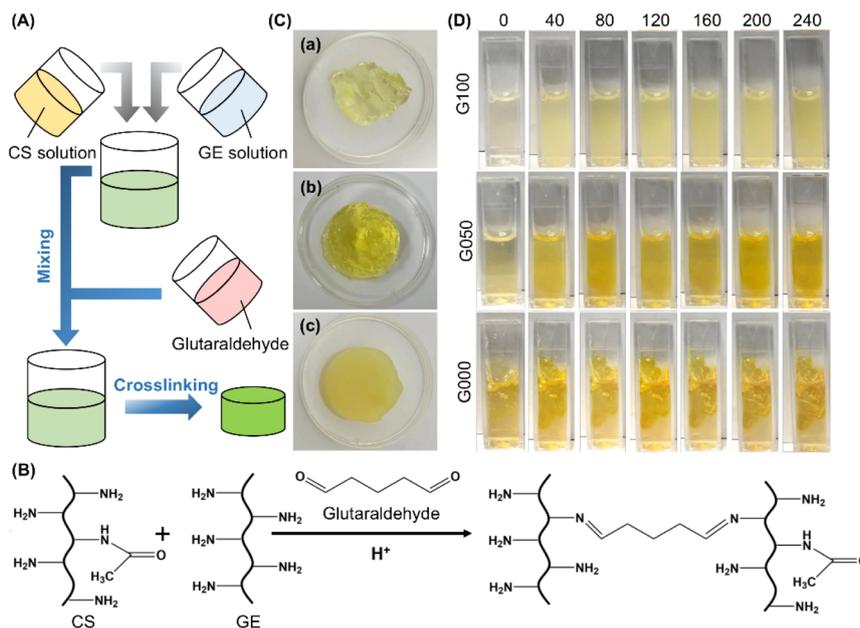| Gel	Volume (mL)		
	CS solution	GE solution	Glutaraldehyde
G000	100	0	10
G025	75	25	10
G050	50	50	10
G075	25	75	10
G100	0	100	10

Fig. 1 (A) A schematic diagram depicting the process of gel formation. (B) Schematic representation of the glutaraldehyde-mediated covalent crosslinking reaction held between CS and GE. (C) Photos of (a) G100, (b) G050, and (c) G000. (D) Photos depicting changes in the reaction mixture during the gelation process when different gels are made. The photos are taken at different time intervals (min), which are shown in the top row of the figure.
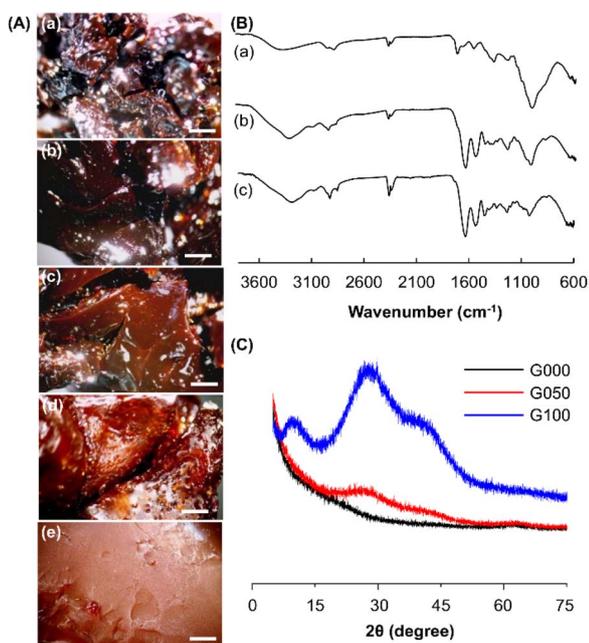

Fig. 2 (A) Microscopic images of gels containing different mass percentages of CS: (a) G000, (b) G025, (c) G050, (d) G075, and (e) G100. Scale bar = 1 mm. (B) FT-IR spectra of (a) G000, (b) G100, and (c) G050. (C) XRD curves of G000, G100 and G050.

2.10 Evaluation of the kinetics of agent release

The release sustainability of a gel was studied using the protocol as previously reported.[22] In brief, 13 g of the agent-loaded gel was put into 30 mL of PBS (pH 7.4). 1 mL of the release medium was withdrawn at regular intervals, and was replenished using the same amount of PBS. The amount of MH released from the MH-loaded gel was measured at λ_{max} of 350 nm using a UV-Vis spectrophotometer. The percentage of cumulative agent release was estimated using the following equation (eqn (3)):

$$\text{Cumulative release}(\%) = \frac{\sum_{t=0}^{t} m_t}{m_\infty} \times 100\% \qquad (3)$$

where m_t is the mass of MH released from the MH-loaded gel at time t, and m_∞ is the total mass of MH loaded into the gel. The release curve was fitted into the zero-order model, the first-order model, the Higuchi model and the Korsmeyer–Peppas model to study the mechanism of agent release.

2.11 Antibacterial test

A G075 gel containing 0.05 g of MH was prepared in a shape of a column (diameter = 1.5 cm, height = 0.2 mm). Either *Staphylococcus aureus* or *Escherichia coli* was swabbed on a LB agar plate. After placing the gel in the plate and incubating the plate for 24 hours at 37 °C, photos were taken. The same procedure was repeated by replacing the MH-loaded gel with a plain gel, a filter paper (circular shape with a diameter of 1.5 cm) soaked with a 0.09% (w/v) NaCl solution, or a filter paper (circular shape with a diameter of 1.5 cm) containing 0.05 g of MH.

2.12 *In vitro* evaluation of toxicity

HEK293 cells and 3T3 mouse fibroblasts were cultured as previously described.[23] 24 hours before the experiment, the cells
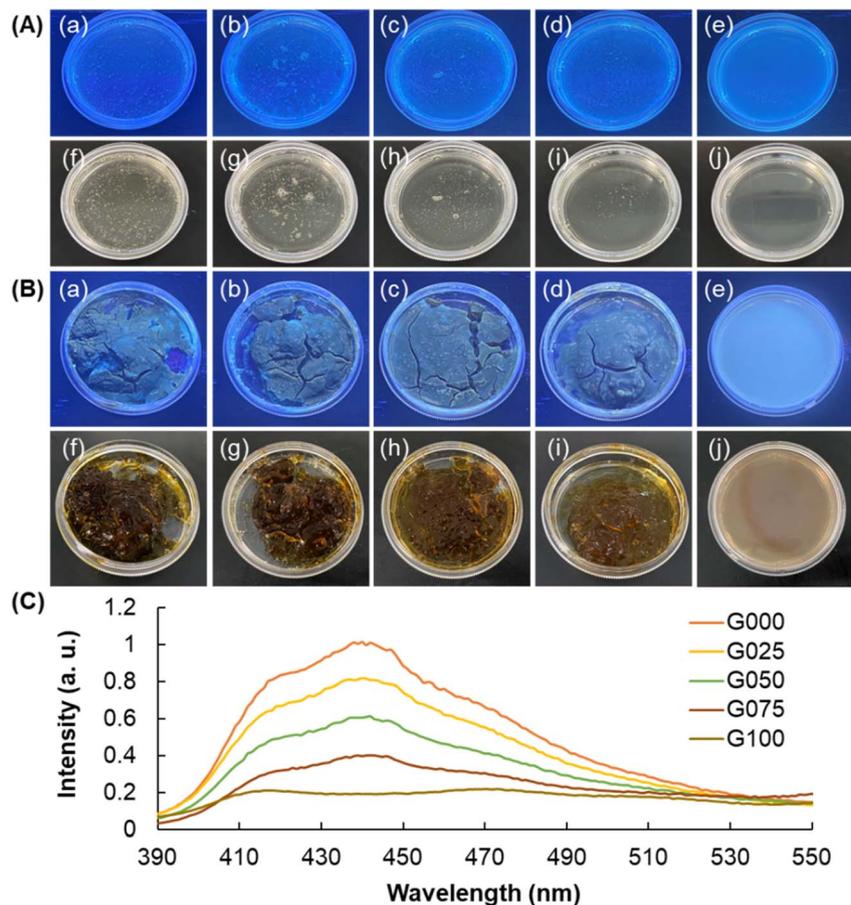
Fig. 3 Optical images of different blended hydrogels [(a, f) G000, (b, g) G025, (c, h) G050, (d, i) G075, and (e, j) G100] under (a, b, c, d, e) UV light and (f, g, h, i, j) white light (A) before and (B) after the cross-linking process. The wavelength of UV light used for excitation is 365 nm. (C) PL spectra of gels containing different mass percentages of CS. The spectra were taken at an excitation wavelength of 365 nm.

were seeded in 96-well plates at a density of 5000 cells per well. The plates were put under a humidified atmosphere of 5% CO_2 at 37 °C. An appropriate amount of CS, GE, or lyophilized gels (including G100, G050 and G000) was ground in the fresh cell culture medium using mortar and pestle to obtain a suspension with a desired concentration. The suspension was then filtered by using a microfilter with the pore size of 0.45 μm. During the assay, the medium in each well was replaced with 100 μL of the filtrate. After 5 hour incubation at 37 °C under a humidified atmosphere of 5% CO_2, the medium in each well was replaced with the fresh cell culture medium. The viability of cells in each well was examined by using the CellTiter 96 Aqueous Non-Radioactive Cell Proliferation Assay (MTS assay; Promega Corp., Madison, WI), according to the manufacturer's instructions, either immediately or after 24 hours of post-treatment incubation.

3. Results and discussion

3.1 Fabrication and structural characterisation of the blended gels

Glutaraldehyde is one of the most commonly used crosslinking agent.[24–29] It is inexpensive and easily available, and has high

efficiency in stabilizing collagenous materials.[30–34] The cross-linking process is mediated by the reaction between the free amino groups of the collagenous materials and the aldehyde groups of GTA. In this study, glutaraldehyde is adopted as a cross-linker to generate hydrogels from CS and GE (Fig. 1A–C). CS is selected to modify the properties and performance of the GE-based hydrogel partly because of its low toxicity, high biocompatibility, high biodegradability, and non-allergenicity.[35] Comparing with the plain GE solution, solutions containing CS form much more heterogeneous gels, with the level of heterogeneity being positively related to the concentration of CS (Fig. 1D). This may be explained by the increase in the viscosity of the gel-forming solution, thereby reducing the efficiency of mixing between the solution and glutaraldehyde. The positive relationship between the extent of heterogeneity of the gel and the mass percentage of CS is further supported by microscopic examination of the generated gels under a stereomicroscope (Fig. 2A). Comparing with G100 which shows a uniform and smooth morphological structure, those containing CS exhibit rough morphological features. The extent of roughness increases when the mass percentage of CS in the gel increases from 25% to 100%. This evidences the impact of increasing the concentration of CS on the efficiency of mixing

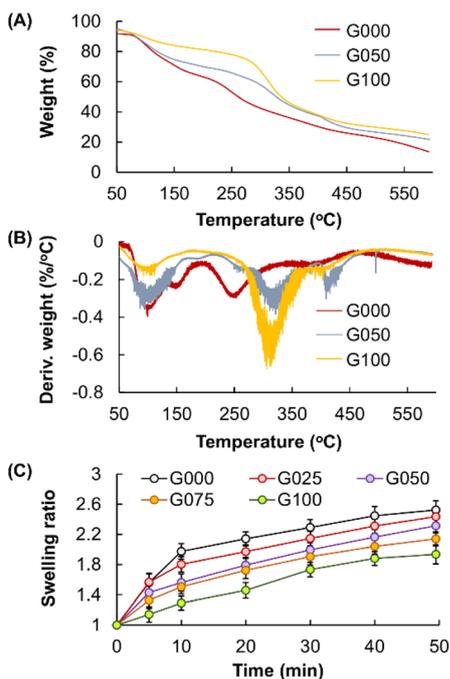© 2023 The Author(s). Published by the Royal Society of Chemistry

Fig. 4 (A) TGA and (B) DTG curves of G000, G050 and G100. (C) Changes in the swelling ratio of the blended gels containing different mass percentages of CS over time.
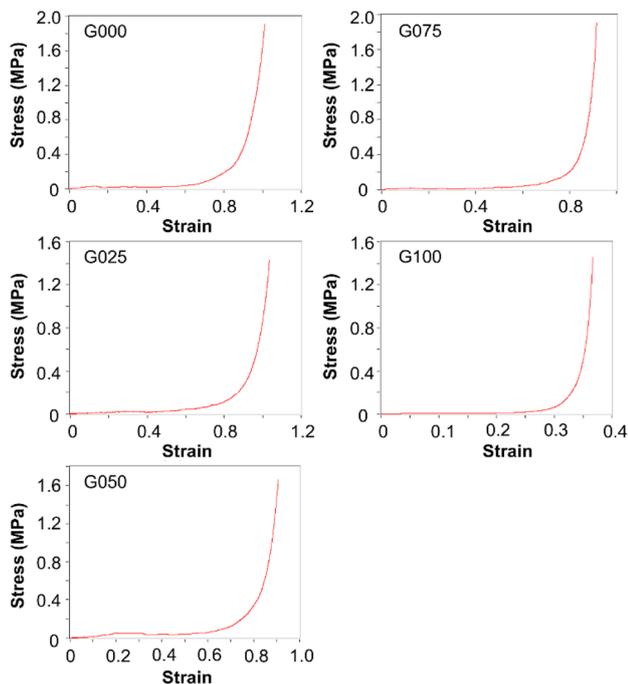

Fig. 5 Compressive stress–strain curves of the blended gels containing different mass percentages of CS.

between the gel-forming solution and the cross-linker, leading to a decline in the homogeneity of the gel structure.

The structures of GE, CS and the gels formed are studied by using FT-IR spectroscopy (Fig. 2B). In the spectrum of GE, a peak is detected at around 1630 cm^{-1}. The presence of this

amide I band is caused by C=O stretching vibrations of the amide group. A signal is also noted at 1539 cm^{-1}. It is assigned to N–H bending vibrations and C–H stretching vibrations. On the other hand, the spectrum of CS exhibits a broad peak at 2960–3599 cm^{-1} owing to O–H and N–H stretching vibrations. Because of C–H and C–N stretching vibrations, a signal is detected at 2879 cm^{-1}. This peak is also present in the spectrum of G050. Structural characterization of the gels is further performed by using the XRD technique. Compared to G000, G100 shows a higher level of crystallinity. The peaks found in G100 also appear in the diffractogram pattern acquired on G050 (Fig. 2C). This suggests that the structural features of both G000 and G100 are retained during the fabrication of G050.

3.2 Self-indicating capacity of the blended gels during gel preparation

GE and CS are known to exhibit clusteroluminogenic properties.[7] In fact, while the photophysics of clusteroluminescence has been studied widely only very recently, the application potential of this optical properties has already been shown in food and pharmaceutical applications.[6,36] Over the years, various mechanisms have been proposed to explain the emissive properties of clusteroluminogenic polymers. Some studies have attributed the luminescence to the oxidation of nitrogen atoms in polymers that contain amine groups;[37,38] while others have linked clusteroluminescence to through-space nonbonding interactions between second and third row heteroatoms.[39–41] In the latter, through-space nonbonding interactions are thought to play a role in producing orbitals that help narrow the energy gap between the HOMO and LUMO of the system.[42]

In this study, the clusteroluminogenic property of the blended gels is shown in Fig. 3. Clusteroluminescence exhibited by the CS solution, GE solution, and CS/GE mixtures is negligible; however, upon the process of cross-linking, the intensity of luminescence increases. This is partly attributed to the fact that the cross-linking process reduces intermolecular distances between polymer chains, facilitating the occurrence of through-space nonbonding interactions. By increasing the mass percentage of CS, the compactness of the gel structure also increases, leading to an increase in the intensity of clusteroluminescence. Regarding the fact that the intensity of luminescence is positively related to the extent of clusterization exhibited by polymer chains, the uniformity of the intensity reflects the homogeneity of the gel structure. For this, we can determine the heterogeneity of the gel during gel preparation in real time by monitoring the uniformity of the intensity of clusteroluminescence exhibited by the gel. In fact, the extent of homogeneity of the luminescence intensity can reflect the extent of homogeneity of the composition of the generated gel, and hence the quality of the gel prepared. Because the homogeneity of the composition of the gel will directly affect drug delivery properties including drug release sustainability and encapsulation efficiency, the clusteroluminogenic properties of the gel serves as an indicator to enable real-time quality control of the blended hydrogel for subsequent bioactive agent delivery applications.
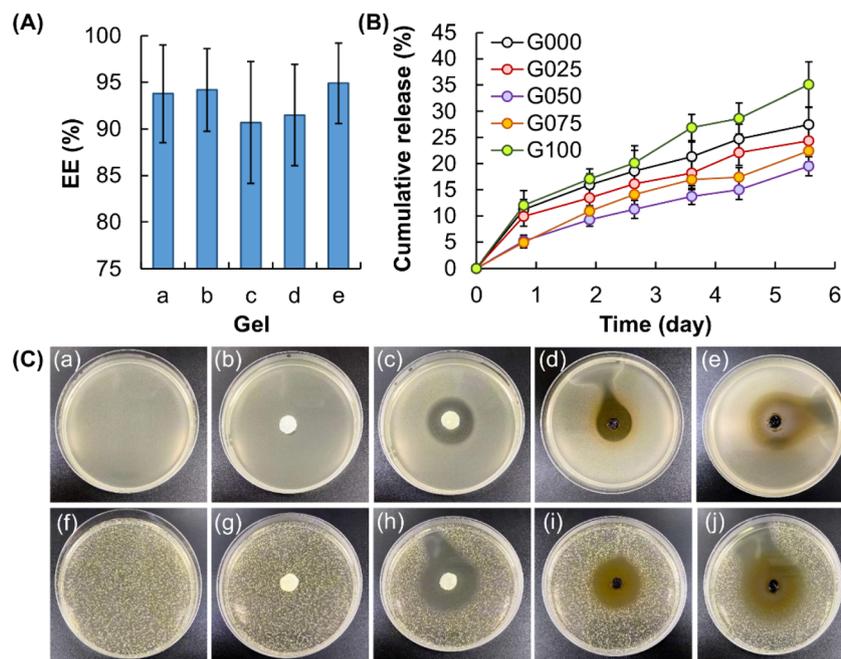
—

Fig. 6 (A) EE of (a) G000, (b) G025, (c) G050, (d) G075, and (e) G100. (B) Release profiles of MH from MH-loaded gels containing different mass percentages of CS. (C) Images showing (a, f) untreated LB plates, as well as the zone of inhibition induced by (b, g) filter paper soaked with an NaCl solution, (c, h) filter paper containing MH, (d, i) plain G075 gel, and (e, j) MH-loaded G075 gel for (a–e) *E. coli* and (f–j) *S. aureus*.

Table 2 Correlation coefficients (r^2) and release exponent (n) of different models for the kinetic data of agent release

Model		Gel				
		G000	G025	G500	G075	G100
Zero-order model	r^2	0.801	0.823	0.940	0.935	0.902
First-order model	r^2	0.860	0.868	0.957	0.957	0.943
Higuchi model	r^2	0.997	0.992	0.968	0.962	0.980
Korsmeyer–Peppas model	n	0.484	0.506	0.683	0.687	0.611
	r^2	0.997	0.992	0.993	0.989	0.991

3.3 Thermal and mechanical properties of the blended gels

The thermal properties of GE, CS, as well as the gels formed, are characterised by using TGA and DTG (Fig. 4A and B). The curve of G100 displays two stages of weight loss. The first stage is observed below 198 °C, accounting for a weight loss of around 18.7%. This weight loss step is caused by the loss of adsorbed moisture. The second stage is found at the temperature range of 215–482 °C, resulting in a weight loss of approximately 50%. In the curve of G000, a significant weight-loss stage also occurs at around 40–167 °C due to the evaporation of physically absorbed or bound water. Another weight loss step is found at the onset temperature of 215 °C, owing to the onset of chain degradation of CS. All these peaks overlap in the curve of G050, leading to a complicated thermal degradation process.

In addition, changing the mass percentage of CS in the blended gels appears to lead to changes in the swelling capacity of the gels (Fig. 4C). The swelling capacity of the gels increases when the mass percentage of CS increases, with C000 showing

the highest swelling capacity. This is attributed to the fact that the presence of CS leads to an increase in the brittleness and rigidity of the gels, facilitating the formation of cracks in the gels during the drying process. The presence of cracks enables more effective diffusion of water molecules into the dried gels, resulting in an increase in the amount of water held by the samples and hence an increase in the determined swelling ratio. Despite this, as demonstrated by the stress–strain curves as presented in Fig. 5, increasing the mass percentage of CS leads to an increase in the overall compressive strength of the gels. This is due to the fact that CS is rich in amine groups.[43–45] Its presence can increase the number of cross-links among polymeric chains. Because the elongation at break of the gels is linked to the breakage of the polymer chains,[46] increasing the mass percentage of CS has led to an increase in the elongation at break of the gels formed.

3.4 Performance of the blended gels in agent delivery

By using MH as a model agent, the EE of all of the blended gels is estimated to be higher than 90% (Fig. 6A). This reveals the high efficiency of the gels in drug encapsulation. Although the difference in the EE of G000, G025, G050, G075 and G100 is found not to be statistically significant, G050 shows the highest agent release sustainability among the gels tested, followed by G025 and G075 (Fig. 6B). On the other hand, the agent release sustainability of gels containing only CS or GE is much lower than that of blended gels (*viz.*, G025, G050, and G075). This is proposed to be due to the combined effect of (i) the increase in the compressive strength of the gels upon the addition of CS and (ii) the ability of GE to form gels with a more compact and
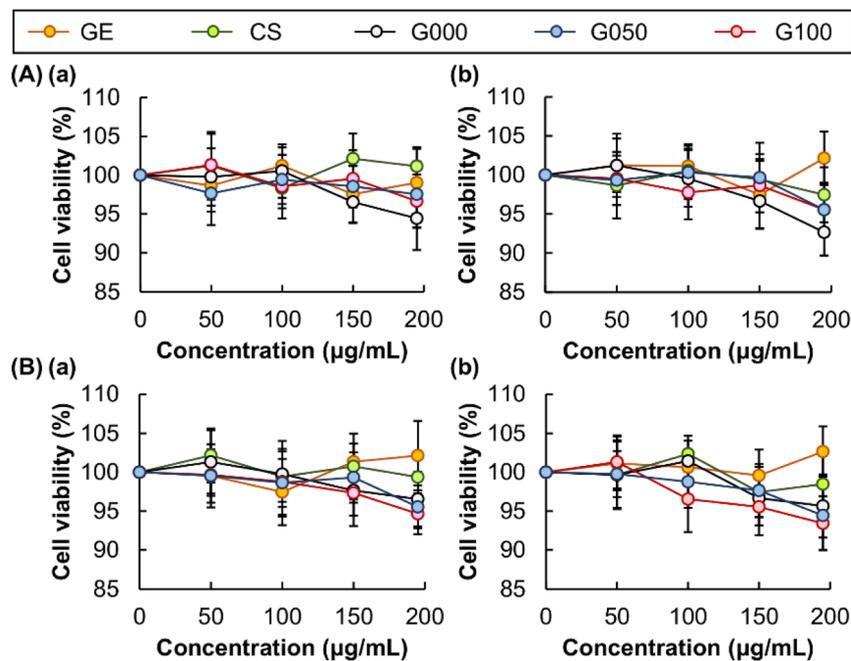
Fig. 7 Viability of (A) 3T3 fibroblasts and (B) HEK 293 cells after 5 h treatment with CS, GE and the gels formed, (a) before and (b) after 24 hour post-treatment incubation.

uniform structure. Upon fitting the curves of agent release into different kinetic models (including the zero-order model, the first-order model, the Higuchi model and the Korsmeyer–Peppas model) and as shown by the calculated regression coefficient (r^2) values (Table 2), the release profiles of the agent-loaded gels are found to fit the Higuchi model the most. This reveals that agent release from the gels involves the penetration of the release medium into the gel matrix. Moreover, the release exponents (n), as calculated by using the Korsmeyer–Peppas equation, are 0.484, 0.506, 0.683, 0.687 and 0.611 for G000, G025, G050, G075 and G100, respectively. This suggests that the release of MH from the gels is mediated mainly *via* non-Fickian diffusion, with the polymer relaxation time being roughly equal to the characteristic solvent diffusion time.[47] For this, the release profiles of MH from the MH-loaded gels are expected to be affected by not only the swelling capacity of the gels but also other factors such as polymer/solvent couple viscoelastic properties.[48]

The retention of the activity of MH after being loaded into the blended gels is evaluated by using *Staphylococcus aureus* (Gram-positive bacteria) and *Escherichia coli* (Gram-negative bacteria) as models. As shown in Fig. 6C, incubation with a filter paper containing 0.05 g of MH leads to the formation of a zone of inhibition in both *Staphylococcus aureus* and *Escherichia coli*. This is attributed to the fact that MH is a semi-synthetic tetracycline derivative displaying broad-spectrum antibiotic activity against Gram-positive and Gram-negative bacteria.[49] In addition, a zone of inhibition is found in both Gram-positive and Gram-negative bacterial treated with plain G075. This is partly explained by the intrinsic antibacterial properties of CS,[50] which enables the plain gel to inhibit bacterial growth. After the gel is loaded with MH, the

antibacterial capacity of the gel is found to be much higher than plain G075. This is due to the combined effects of MH and the intrinsically antibacterial properties of the gel, and evidences the retention of the activity of MH after the agent loading process.

3.5   Toxicity of the blended gels

While the release sustainability and EE are important factors to be considered when a material is adopted for bioactive agent delivery, low toxicity of the material is required for real applications.[51–53] The toxicity of CS and GE is examined *in vitro* by using the MTS assay (Fig. 7). No significant loss of cell viability is detected after 5 hour treatment with both agents. This indicates that no apparent cytotoxicity is mediated by CS or GE. To evaluate the possible occurrence of delayed onset of cytotoxicity after treatment, the viability of the treated cells is examined after 24 hour post-treatment incubation. No observable cytotoxicity is found in all concentrations tested. This suggests the high safety profiles of the ingredients used for gel fabrication. Apart from examining the cytotoxicity of CS and GE, we examine the cytotoxic effects brought about by the gels formed. Loss of cell viability is negligible after treatment with different gels, regardless of the presence or absence of 24 hour post-treatment incubation. This demonstrates that cytotoxicity caused by the gels is acceptable.

4.   Concluding remarks

Hydrogels have been extensively exploited as carriers of bioactive agents,[54,55] with the performance in bioactive agent delivery being significantly affected by how the gels are fabricated and

handled. In this study, GE and CS, which are two biopolymers that have been extensively adopted for applications in biomedicine,[56–61] have been adopted to generate blended hydrogels that not only allow for sustained agent release but also effectively retain the bioactivity of the loaded agent. In addition, the presence of CS renders the blended gels intrinsically antibacterial in nature. Importantly, owing to their clusteroluminogenic properties, the gels show self-indicating capacity that enable real-time quality control of the generated gels during gel preparation. Along with the negligible chronic and acute toxicity of the gels as demonstrated in the *in vitro* context, our gels show the potential to be further exploited for use as smart sustained-release carriers of bioactive agents.

Author contributions

WFL designed the research work, supervised the research, revised the manuscript, and wrote the manuscript. WFL, OSR, LL, and HW collected the data. WFL and WTW reviewed the manuscript. All authors read and approved the final manuscript.

Conflicts of interest

The authors declare that they have no conflicts of interest. The funder had no role in the design of the study; in the collection, analyses, or interpretation of data; in the writing of the manuscript, or in the decision to publish the results.

Acknowledgements

References

1 Y. Chen, J. Li, J. Lu, M. Ding and Y. Chen, *Polym. Test.*, 2022, **108**, 107516.

2 J. Lu, Y. Chen, M. Ding, X. Fan, J. Hu, Y. Chen, J. Li, Z. Li and W. Liu, *Carbohydr. Polym.*, 2022, **277**, 118871.

3 W. F. Lai, A. L. Rogach and W. T. Wong, *Composites, Part A*, 2018, **113**, 318–329.

4 W. F. Lai and A. L. Rogach, *ACS Appl. Mater. Interfaces*, 2017, **9**, 11309–11320.

5 W. F. Lai and Z. D. He, *J. Controlled Release*, 2016, **243**, 269–282.

6 W. F. Lai, R. Deng, T. C. He and W. T. Wong, *Adv. Healthcare Mater.*, 2021, **10**, 2170006.

7 W. F. Lai, *Mater. Today Chem.*, 2022, **23**, 100712.

8 O. Madkhali, G. Mekhail and S. D. Wettig, *Int. J. Pharm.*, 2019, **554**, 224–234.

9 M. C. Echave, L. Saenz del Burgo, J. L. Pedraz and G. Orive, *Curr. Pharm. Des.*, 2017, **23**, 3567–3584.

10 M. C. Echave, R. Hernaez-Moya, L. Iturriaga, J. L. Pedraz, R. Lakshminarayanan, A. Dolatshahi-Pirouz, N. Taebnia and G. Orive, *Expert Opin. Biol. Ther.*, 2019, **19**, 773–779.

11 K. Yue, G. Trujillo-de Santiago, M. M. Alvarez, A. Tamayol, N. Annabi and A. Khademhosseini, *Biomaterials*, 2015, **73**, 254–271.

12 W. Treesuppharat, P. Rojanapanthu, C. Siangsanoh, H. Manuspiya and S. Ummartyotin, *Biotechnol. Rep.*, 2017, **15**, 84–91.

13 S. S. Sagiri, V. K. Singh, S. Kulanthaivel, I. Banerjee, P. Basak, M. K. Battachrya and K. Pal, *J. Mech. Behav. Biomed. Mater.*, 2015, **43**, 1–17.

14 R. Oun, J. A. Plumb and N. J. Wheate, *J. Inorg. Biochem.*, 2014, **134**, 100–105.

15 M. Jaiswal, A. Gupta, A. K. Agrawal, M. Jassal, A. K. Dinda and V. Koul, *J. Biomed. Nanotechnol.*, 2013, **9**, 1495–1508.

16 R. Jahanban-Esfahlan, H. Derakhshankhah, B. Haghshenas, B. Massoumi, M. Abbasian and M. Jaymand, *Int. J. Biol. Macromol.*, 2020, **156**, 438–445.

17 T. Kobayashi, M. Mizuta, N. Hiwatashi, Y. Kishimoto, T. Nakamura, S. I. Kanemaru and S. Hirano, *Auris, Nasus, Larynx*, 2017, **44**, 86–92.

18 S. K. Bhattacharyya, M. Dule, R. Paul, J. Dash, M. Anas, T. K. Mandal, P. Das, N. C. Das and S. Banerjee, *ACS Biomater. Sci. Eng.*, 2020, **6**, 5662–5674.

19 J. K. Suh and H. W. Matthew, *Biomaterials*, 2000, **21**, 2589–2598.

20 W. Paul and C. P. Garside, *STP Pharma Sci.*, 2000, **10**, 5–22.

21 W. F. Lai, C. Hu, G. Deng, K. H. Lui, X. Wang, T. H. Tsoi, S. Wang and W. T. Wong, *Int. J. Pharm.*, 2019, **566**, 101–110.

22 W. F. Lai, E. Huang and W. T. Wong, *Appl. Mater. Today*, 2020, **21**, 100876.

23 W. F. Lai, A. S. Susha, A. L. Rogach, G. A. Wang, M. J. Huang, W. J. Hu and W. T. Wong, *RSC Adv.*, 2017, **7**, 44482–44491.

24 D. Tahtat, M. Mahlous, S. Benamer, A. N. Khodja, H. Oussedik-Oumehdi and F. Laraba-Djebari, *Int. J. Biol. Macromol.*, 2013, **58**, 160–168.

25 V. K. Sharma, P. P. Sharma, B. Mazumder, A. Bhatnagar and T. Singh, *Curr. Drug Delivery*, 2015, **12**, 693–702.

26 V. K. Sharma, P. P. Sharma, B. Mazumder, A. Bhatnagar, V. Subramaniyan, S. Fuloria and N. K. Fuloria, *J. Biomater. Sci., Polym. Ed.*, 2021, **32**, 1420–1449.

27 M. Nouri-Felekori, M. Khakbiz, N. Nezafati, J. Mohammadi and M. B. Eslaminejad, *Int. J. Pharm.*, 2019, **557**, 208–220.

28 S. Mallakpour and S. Rashidimoghadam, *Int. J. Biol. Macromol.*, 2020, **144**, 389–402.

29 L. X. Gao, J. L. Chen, X. W. Han, S. X. Yan, Y. Zhang, W. Q. Zhang and Z. W. Gao, *J. Biomater. Sci., Polym. Ed.*, 2015, **26**, 545–557.

30 A. D. Russell, *Infect. Control Hosp. Epidemiol.*, 1994, **15**, 724–733.

31 M. Rusmah, *Singapore Dent. J.*, 1993, **18**, 17–21.

32 D. Romano-Woodward, *Nurs. Stand.*, 2000, **14**, 47–51.

33 A. Jayakrishnan and S. R. Jameela, *Biomaterials*, 1996, **17**, 471–484.

34 L. Abbott, *Occup. Health Nurs.*, 1995, **47**, 238–239.

35 S. K. Kim and N. Rajapakse, *Carbohydr. Polym.*, 2005, **62**, 357–368.

36 W. F. Lai and W. T. Wong, *Membranes*, 2022, **12**, 437.

37 C. C. Chu and T. Imae, *Macromol. Rapid Commun.*, 2009, **30**, 89–93.

38 D. Wang, T. Imae and M. Miki, *J. Colloid Interface Sci.*, 2007, **306**, 222–227.

39 X. G. Guo, J. Quinn, Z. H. Chen, H. Usta, Y. Zheng, Y. Xia, J. W. Hennek, R. P. Ortiz, T. J. Marks and A. Facchetti, *J. Am. Chem. Soc.*, 2013, **135**, 1986–1996.

40 N. Hergue, C. Mallet, G. Savitha, M. Allain, P. Frere and J. Roncali, *Org. Lett.*, 2011, **13**, 1762–1765.

41 A. S. Ozen, C. Atilgan and G. Sonmez, *J. Phys. Chem. C*, 2007, **111**, 16362–16371.

42 R. Hoffmann, *Acc. Chem. Res.*, 1971, **4**, 1–9.

43 Z. G. Wang, Y. E. Shi, X. M. Yang, Y. Xiong, Y. X. Li, B. K. Chen, W. F. Lai and A. L. Rogach, *Adv. Funct. Mater.*, 2018, **28**, 1802848.

44 W. F. Lai and H. C. Shum, *ACS Appl. Mater. Interfaces*, 2015, **7**, 10501–10510.

45 W. F. Lai and M. C. Lin, *Curr. Gene Ther.*, 2015, **15**, 472–480.

46 Q. W. Tang, X. M. Sun, J. H. Wu, Q. H. Li and J. M. Lin, *Polym. Eng. Sci.*, 2009, **49**, 1871–1878.

47 B. Chanabodeechalermrung, T. Chaiwarit, S. R. Sommano, P. Rachtanapun, N. Kantrong, C. Chittasupho and P. Jantrawut, *Membranes*, 2022, **12**, 825.

48 G. Mario and G. Gabriele, *Curr. Drug Delivery*, 2005, **2**, 97–116.

49 W. F. Lai, E. Wong and W. T. Wong, *RSC Adv.*, 2020, **10**, 44522–44532.

50 W. F. Lai, S. Y. Zhao and J. C. Chiou, *Carbohydr. Polym.*, 2021, **271**, 118447.

51 J. Li, J. Zhao, T. Tan, M. Liu, Z. Zeng, Y. Zeng, L. Zhang, C. Fu, D. Chen and T. Xie, *Int. J. Nanomed.*, 2020, **15**, 2563–2582.

52 R. Yang, E. Hou, W. Cheng, X. Yan, T. Zhang, S. Li, H. Yao, J. Liu and Y. Guo, *J. Med. Chem.*, 2022, **65**, 16879–16892.

53 C. Y. Gong, Q. J. Wu, P. W. Dong, S. Shi, S. Z. Fu, G. Guo, H. Z. Hu, X. Zhao, Y. Q. Wei and Z. Y. Qian, *J. Biomed. Mater. Res., Part B*, 2009, **91**, 26–36.

54 W. F. Lai and H. C. Shum, *Nanoscale*, 2016, **8**, 517–528.

55 W. F. Lai, A. S. Susha and A. L. Rogach, *ACS Appl. Mater. Interfaces*, 2016, **8**, 871–880.

56 N. Sahoo, R. K. Sahoo, N. Biswas, A. Guha and K. Kuotsu, *Int. J. Biol. Macromol.*, 2015, **81**, 317–331.

57 R. M. Hathout and M. K. Omran, *Pharm. Dev. Technol.*, 2016, **21**, 379–386.

58 M. Foox and M. Zilberman, *Expert Opin. Drug Delivery*, 2015, **12**, 1547–1563.

59 K. Dua, M. Bebawy, R. Awasthi, R. K. Tekade, M. Tekade, G. Gupta, T. De Jesus Andreoli Pinto and P. M. Hansbro, *Pharm. Nanotechnol.*, 2017, **5**, 243–249.

60 A. Ali and S. Ahmed, *Int. J. Biol. Macromol.*, 2018, **109**, 273–286.

61 S. M. Ahsan, M. Thomas, K. K. Reddy, S. G. Sooraparaju, A. Asthana and I. Bhatnagar, *Int. J. Biol. Macromol.*, 2018, **110**, 97–109.